Available online at www.sciencedirect.com
SCIENCE DIRECT®
Journal of Sound and Vibration 268 (2003) 49–70
JOURNAL OF SOUND AND VIBRATION
www.elsevier.com/locate/jsvi

System mode approach for analysis of horizontal vibration of 3-D two-link flexible manipulators

Joono Cheong, Youngil Youm*

Department of Mechanical Engineering, Pohang University of Science and Technology (POSTECH), San 31, Hyoja-dong, Pohang 790-784, South Korea

Received 5 December 2001; accepted 5 November 2002

Abstract

This paper deals with the system mode analysis of horizontal vibration for 3-D two-link flexible manipulators. For the analysis, we formulate and solve a set of partial differential equations which represent vibration mixed with bending and torsional moment. The inclusion of torsional vibration complicates the analysis, but the results are more precise and realistic. We obtain a number of geometrical and dynamical boundary conditions depending on manipulator configuration. There are two possible boundary conditions at the rotary joint: clamped and pinned with spring condition. We perform a examination and comparison between the two joint conditions. Numerical and experimental tests show the validity and effectiveness of the proposed analysis and modelling.

1. Introduction

Precise modelling of vibration in a flexible structure is the fundamental step toward sophisticated vibration control. So far, the vibrations of links in most of the flexible robots have been modelled by the assumed mode solutions of each flexible link (i.e., component mode of each link). They need a large number of mode solutions and many degrees of freedoms so that the modellings are accurate enough. The component modes of vibration, which originally contain the local nature of each link, are combined together to yield system mode of vibration. Oakley [1] stated that a larger dimension of component modes is needed to obtain a certain dimension of system modes. Consequently, a greater dimensional eigenvalue decomposition has to be solved, but it is too time-consuming to compute on-line. In addition, the resulting system mode shapes

*Corresponding author. Fax: +82-54-279-5899.
E-mail address: youm@postech.ac.kr (Y. Youm).

0022-460X/03/$ - see front matter
doi:10.1016/S0022-460X(02)01474-8

after eigenvalue decomposition may be erroneous due to inexact boundary conditions. A few papers deal with the analysis of system mode vibration of two connected flexible members. The exact system mode of L-shaped flexible structure was studied by Bang [2]. Milford and Asokanthan [3] discussed the analysis of system mode vibration of planar two-link flexible robot, directly solving partial differential equations. For simplicity, they assumed each rotary joint as the clamped boundary. More detailed and completed work was done by Cheong et al. [4]. In their work, four possible sets of joint boundary conditions were investigated. To model the boundary condition of each joint, the spring-hinged condition was included in parallel with clamped condition. This enables us to observe the effect of joint servo gain, similarly done by Garcia and Inman [5], and Cetinkunt and Yu [6].

Until now, the analysis of system mode vibration of 3-D flexible robots shown in Fig. 1 has not been studied. Apparently, the geometric joint workspace may be decomposed into horizontal and vertical planes at the instant as shown in Ref. [7]. The 3-D vibration of the robot is also decomposed in a similar way. We define the vertical vibration to be the vibration that occurred by the rotation of joint 2 and/or joint 3, while the horizontal vibration occurred solely by the rotation of joint 1. For system mode analysis of the vertical vibration, one can directly apply the results of two-link flexible robots moving in a plane in Refs. [3,4]. Hence, if the analysis of horizontal vibration has been performed, we will have completed the analysis for the system mode vibration of 3-D vibration. An interesting feature of the horizontal vibration is that it incorporates torsional vibration. This is caused by the geometric asymmetry about the longitudinal axis of the upper

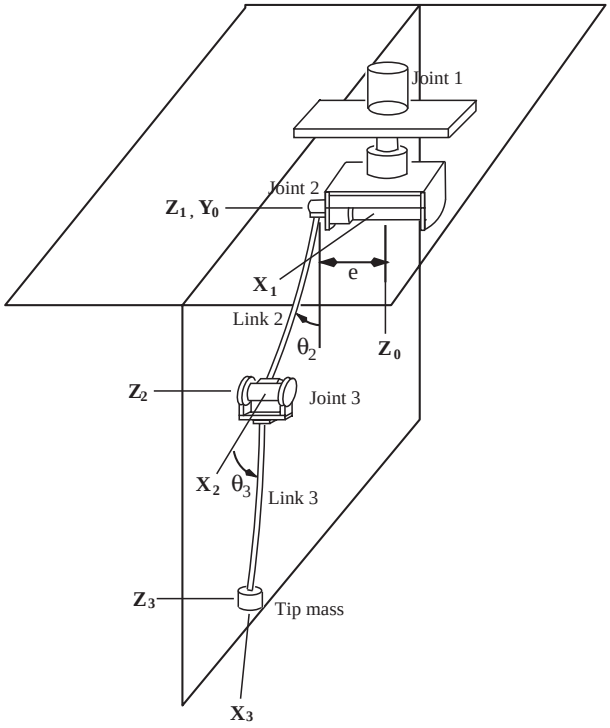

Fig. 1. Schematic of 3-D flexible manipulator.

link. Research works related with coupled bending-torsional problems can be found in Ref. [8], where the torsional moment due to the asymmetry of the lumped mass at the tip was treated in a single link flexible robot, and in Ref. [9], where the estimation of 3-D vibration including torsion in a multi-link robot was studied using the component mode analysis. Practical examples of horizontal motion with horizontal vibration can be found in other applications like the tower crane and the pump car. The slender booms or pipes of those machines produce vibrations when they undergo horizontal motions. If we have accurate knowledge about the characteristics of the horizontal vibration, we can speed up tasks and increase productivity by a proper control of the vibration.

In this paper, we will solve the horizontal vibration of a 3-D two-link robot; we will use the extended Hamilton's principle to derive the governing equations and the corresponding boundary conditions. After setting up the equations, the system mode analysis will be carried out. The coupling effect between bending and torsion is also fully studied. The outline of this paper is as follows: Modelling and notation necessary for subsequent development are described in Section 2. Section 3 is devoted to the analysis of the system mode of horizontal vibration. Numerical and experimental results are given in Sections 4 and 5, respectively. Finally, conclusions are presented in Section 6.

2. Modelling

Consider a 3-D manipulator with two flexible links as shown in Fig. 1, where e denotes shoulder offset. As defined in the previous section, the decomposition of the 3-D vibration into vertical and horizontal vibration makes the analysis easy. Note that the horizontal vibration may have vertical components of displacement in Cartesian space due to the torsional motion. However, since the torsional motion always combined with horizontal rotation, we conveniently consider the vibration from the horizontal rotation as the horizontal vibration. On the other hand, the vertical vibration remains only in the vertical motion plane.

In conventional modelling, the horizontal and vertical vibrations of each link are mathematically described by the summation of assumed component modes such that

$$y_i(x_i,t)=\sum_{k=1}^{m_i}\psi_{i,k}(x_i)r_{i,k}(t),\quad i=2,3,\qquad v_i(x_i,t)=\sum_{k=1}^{m_i}\phi_{i,k}(x_i)s_{i,k}(t),\quad i=2,3, \tag{1}$$

where y_i and v_i are the horizontal and vertical vibrations, respectively, and i and k denote link number and mode number, respectively. m_i is the number of vibration modes in the ith link. The first link is rigid, so the two flexible links are numbered as the second and the third links. $\psi_{i,k}(x_i)$ and $\phi_{i,k}(x_i)$ are mode shape functions of horizontal and vertical vibration, $r_{i,k}(t)$ and $s_{i,k}(t)$ are their corresponding time functions, and x_i is the domain of the ith link such that $0\leqslant x_i\leqslant L_i$, where L_i is the length of the ith link. From the structure of the flexible robot in Fig. 1, it can be written as

$$\theta_h\triangleq\theta_1,\quad \boldsymbol{\theta}_v\triangleq[\theta_2\quad\theta_3]^{\mathrm{T}},\quad \tau_h\triangleq\tau_1,\quad \boldsymbol{\tau}_v\triangleq[\tau_2\quad\tau_3]^{\mathrm{T}},$$

where h and v represent variables related with horizontal and vertical subspaces. According to a physical observation, the natural frequencies and mode shapes of both subsystems are changing mainly according to the variation of the elbow joint θ_3.

In an accurate modelling, the assumed mode expansion up to finite numbers may fail to describe a real vibration in wide range of configurations due to inexact boundary conditions and discontinuity at the interconnection of flexible links. Also, we have no systematic way to determine how many modes are included to describe actual vibration accurately. The use of the system mode description will eliminate these problems. In this paper, our major concern will be the analysis of the horizontal vibration in a completely analytic way.

3. Horizontal system mode analysis

Fig. 2 illustrates the definitions of horizontal vibration using the component mode description and the system mode description; in the component mode description, the vibration of each link is defined only along the side of each link, but in the system mode description, the vibration is defined over the whole body. The advantage of the component modes is that they can be solved easily or simply obtained from engineering handbooks. The disadvantage is that they are liable to give inaccurate composite modes when they are fused together by the eigenvalue decomposition. Moreover, the eigenvalue decomposition takes large computation time; as the dimension increases, the eigenvalue problem takes much more time. We cannot avoided the eigenvalue decomposition procedures if the component mode description is applied at the modelling step. The system mode description is much better in obtaining more accurate vibration modes even if it is a little complicated to formulate and solve. Also, using the system mode description, we can approximate the vibration precisely with a lower number of modes without the eigenvalue decomposition.

In general 3-D robot systems, the horizontal and vertical motions appear simultaneously in 3-D space. This makes it difficult for us to simply decompose 3-D motion into pure vertical and horizontal motions; they are coupled with each other. However, fortunately, the only coupling terms between the two plane motions are velocity terms. When we linearize the system about an

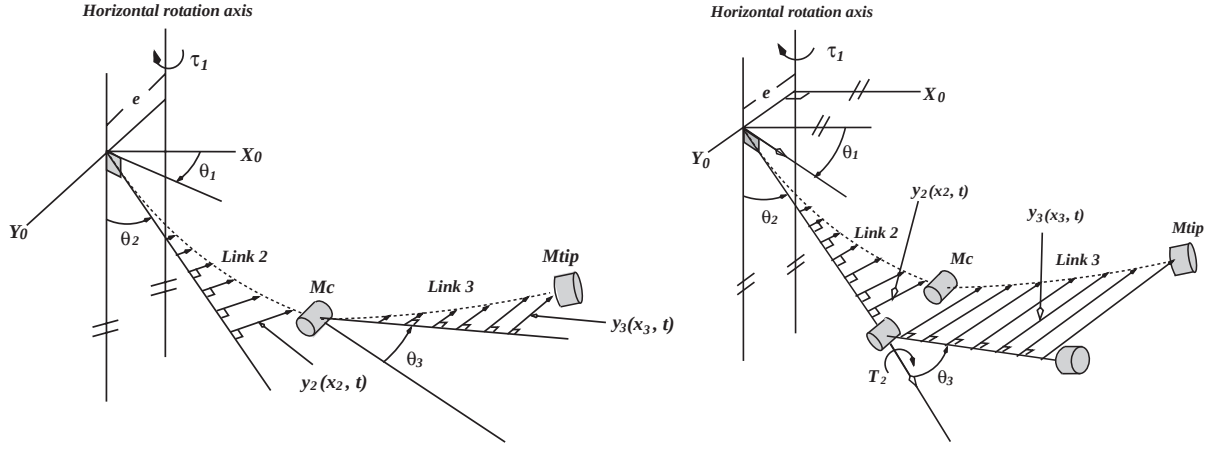

(a) Component mode (b) System mode

Fig. 2. Definitions of horizontal vibration.

operating point where all the velocity terms are zero, two motions can be decoupled. Actually, the coupling force do not contribute the natural modes of vibration, and it can be definitely interpreted as the non-linear forcing terms acting on each linear vibration system. Another thing to note is that the effect of torsional vibration appears during the horizontal rotation. The torsion does not arise during the pure vertical motion. Since it is combined with the horizontal bending deflection, this makes the deflection more severe. The effect of the torsional vibration increases when the relative angle θ_3 between two links are large. Fig. 3 depicts the effect of torsion to the horizontal vibration. Due to the torsion, the bending deflection of the lower link becomes larger.

3.1. Derivation of equations of motion

The governing equations and the corresponding boundary conditions of the system in Fig. 2(b) can be obtained using the extended Hamilton's principle [10]. According to the Hamilton's principle, the Lagrangian and non-conservative work have the following relation for arbitrary time t_1 and t_2:

$$\int_{t_1}^{t_2} (\delta \mathscr{L} - \delta \mathscr{W}_{nc})\, \mathrm{d}t, \tag{2}$$

where $\mathscr{L} = \mathscr{K} - \mathscr{P}$ and $\mathscr{W}_{nc}$ are the Lagrangian and work done by external forces, and $\mathscr{K}$ and $\mathscr{P}$ are the kinetic energy and the potential energy, respectively. For developing the governing equations, we make assumptions:

- the joint variables are fixed at a given configuration,
- the effect of should offset is neglected since it is small, and
- the torsional vibration in the lower flexible link is neglected since the majority of the torsional vibration arises in the upper link.

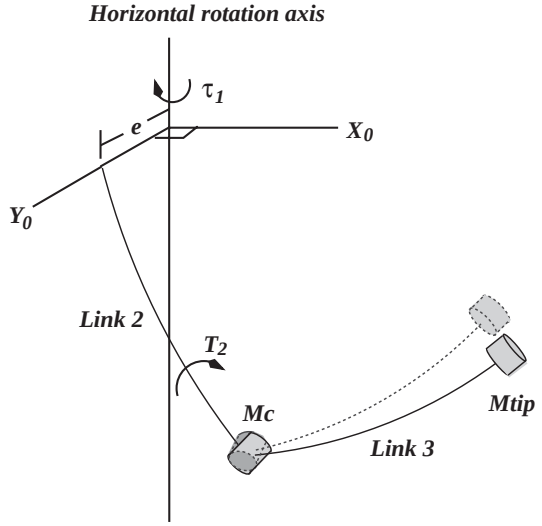

Fig. 3. Effect of torsional deflection.

First we consider the clamped joint case; thus, joint 1 is fixed without motion. The kinetic energy of the horizontal vibration $\mathscr{K}$ is

$$\mathscr{K} = \mathscr{K}_0 + \mathscr{K}_1, \tag{3}$$

where $\mathscr{K}_0$ and $\mathscr{K}_1$ are the portions of kinetic energies by lumped elements and elastic links, respectively, and they are defined as

$$\begin{aligned}\mathscr{K}_0 = &\tfrac{1}{2}M_c(\dot{y}_2(L_2))^2 + \tfrac{1}{2}M_{tip}(\dot{y}_3(L_3))^2 + \tfrac{1}{2}I_c(\dot{y}_2'(L_2))^2 \\ &+ \tfrac{1}{2}I_{tip}(\dot{y}_3'(L_3))^2 + \tfrac{1}{2}J_c(\dot{T}_2(L_2))^2,\end{aligned} \tag{4}$$

$$\mathscr{K}_1 = \frac{1}{2}\int_0^{L_2} \rho_2 \dot{y}_2^2 \,\mathrm{d}x_2 + \frac{1}{2}\int_0^{L_3} \rho_3 \dot{y}_3^2 \,\mathrm{d}x_3 + \frac{1}{2}\int_0^{L_2} b_2 \dot{T}_2^2 \,\mathrm{d}x_2, \tag{5}$$

where y_2 and y_3 are the horizontal bending deflection of links 2 and 3, and T_2 is the torsional deflection of link 2; M_c and M_{tip} are the center mass and tip mass, I_c an I_{tip} are the moment of inertia of the center mass and tip mass in the direction of bending moment, and J_c is the moment of inertia of the total outer body from the center in the direction of the torsional moment—J_c depends on the elbow angle θ_3; ρ_2 and ρ_3 are the density of links 2 and 3, and b_2 is the unit polar moment of inertia of link 2. The dot and prime mean the time derivative and spatial derivative, respectively.

For the potential energy $\mathscr{P}$, we consider the elastic potential energy only such that

$$\mathscr{P} = \frac{1}{2}EI_2\int_0^{L_2}(y_2'')^2 \,\mathrm{d}x_2 + \frac{1}{2}EI_3\int_0^{L_3}(y_3'')^2 \,\mathrm{d}x_3 + \frac{1}{2}GJ_2\int_0^{L_2}(T_2')^2 \,\mathrm{d}x_2, \tag{6}$$

where EI_i is the flexural rigidity of the ith link, and GI_2 is the torsional rigidity of link 2. If we rewrite the Lagrangian as

$$\mathscr{L} = \mathscr{L}_0 + \mathscr{L}_1, \tag{7}$$

where $\mathscr{L}_0 = \mathscr{K}_0$ and $\mathscr{L}_1 = \mathscr{K}_1 - \mathscr{P}$, the Lagrangian density functions for $\mathscr{L}_1$ can be defined:

$$\mathscr{L}_1 = \int_0^{L_2} h_2 \,\mathrm{d}x_2 + \int_0^{L_3} h_3 \,\mathrm{d}x_3 + \int_0^{L_2} g_2 \,\mathrm{d}x_2, \tag{8}$$

where

$$\begin{aligned} h_2 &= \tfrac{1}{2}\rho_2\dot{y}_2^2 - \tfrac{1}{2}EI_2(y_2'')^2, \\ h_3 &= \tfrac{1}{2}\rho_3\dot{y}_3^2 - \tfrac{1}{2}EI_3(y_3'')^2, \\ g_2 &= \tfrac{1}{2}b_2\dot{T}_2^2 - \tfrac{1}{2}GJ_2(T_2')^2, \end{aligned}$$

are the Lagrangian density functions. As for the non-conservative work $\mathscr{W}_{nc}$, we do not have to consider it because there is no external force when we assume the joint boundary to be clamped.The variation of Lagrangian $\mathscr{L}_1$ becomes

$$\begin{aligned}\delta\mathscr{L} &= \delta\mathscr{L}_0 + \delta\mathscr{L}_1 \\ &= \delta\mathscr{L}_0 + \int_0^{L_2}\delta h_2 \,\mathrm{d}x_2 + \int_0^{L_3}\delta h_3 \,\mathrm{d}x_3 + \int_0^{L_2}\delta g_2 \,\mathrm{d}x_2,\end{aligned} \tag{9}$$

where

$$\delta h_2 = \frac{\partial h_2}{\partial \dot{y}_2}\delta \dot{y}_2 + \frac{\partial h_2}{\partial y_2''}\delta y_2'',$$

$$\delta h_3 = \frac{\partial h_3}{\partial \dot{y}_3}\delta \dot{y}_3 + \frac{\partial h_3}{\partial y_3''}\delta y_3'',$$

$$\delta g_2 = \frac{\partial g_2}{\partial \dot{T}_2}\delta \dot{T}_2 + \frac{\partial g_2}{\partial T_2'}\delta T_2'.$$

Performing the integration by parts, $\delta \mathscr{L}_1$ can be rewritten as follows:

$$\begin{aligned}\delta \mathscr{L}_1 = &-\int_0^{L_2}\left[\frac{\partial}{\partial t}\left(\frac{\partial h_2}{\partial \dot{y}_2}\right) - \left(\frac{\partial h_2}{\partial y_2''}\right)''\right]\delta y_2 \,\mathrm{d}x_2 \\ &-\int_0^{L_3}\left[\frac{\partial}{\partial t}\left(\frac{\partial h_3}{\partial \dot{y}_3}\right) - \left(\frac{\partial h_3}{\partial y_3''}\right)''\right]\delta y_3 \,\mathrm{d}x_3 \\ &-\int_0^{L_2}\left[\frac{\partial}{\partial t}\left(\frac{\partial g_2}{\partial \dot{T}_2}\right) + \left(\frac{\partial T_2}{\partial T_2'}\right)'\right]\delta T_2 \,\mathrm{d}x_2 \\ &+\frac{\partial h_2}{\partial y_2''}\delta y_2'\Big|_0^{L_2} - \left(\frac{\partial h_2}{\partial y_2''}\right)'\delta y_2\Big|_0^{L_2} + \frac{\partial h_3}{\partial y_3''}\delta y_3'\Big|_0^{L_3} \\ &-\left(\frac{\partial h_3}{\partial y_3''}\right)'\delta y_3\Big|_0^{L_3} + \frac{\partial g_2}{\partial T_2'}\delta T_2\Big|_0^{L_2}. \end{aligned} \tag{10}$$

In the above, terms inside of each bracket in the first three lines determine the equations of motions, and the other lines determine the boundary conditions in conjunction with $\delta \mathscr{L}_0$ which is written as

$$\begin{aligned}\delta \mathscr{L}_0 = &-\frac{\partial}{\partial t}\left(\frac{\partial \mathscr{L}_0}{\partial \dot{y}_2}\right)\delta y_2(L_2) - \frac{\partial}{\partial t}\left(\frac{\partial \mathscr{L}_0}{\partial \dot{y}_3}\right)\delta y_3(L_3) - \frac{\partial}{\partial t}\left(\frac{\partial \mathscr{L}_0}{\partial \dot{y}_2'}\right)\delta y_2'(L_2) \\ &-\frac{\partial}{\partial t}\left(\frac{\partial \mathscr{L}_0}{\partial \dot{y}_3'}\right)\delta y_3'(L_3) - \frac{\partial}{\partial t}\left(\frac{\partial \mathscr{L}_0}{\partial \dot{T}_2}\right)\delta T_2(L_2). \end{aligned} \tag{11}$$

See Ref. [10] for the derivation of Eq. (11). If we put kinetic and potential energies in Eqs. (4)–(6) into $\delta \mathscr{L}_0$ and $\delta \mathscr{L}_1$, we can get the equations of motions and corresponding boundary conditions after a consider a considerable amount of mathematical manipulation. The equations of motions and boundary conditions are so determined to satisfy Eq. (2) always for arbitrary variations of variables at all boundaries.

From Eq. (10), the equations of motions are

$$EI_2 y_2'''' + \rho_2 \ddot{y}_2 = 0, \tag{12}$$

$$EI_3 y_3'''' + \rho_3 \ddot{y}_3 = 0, \tag{13}$$

$$GJ_2 T_2'' + b_2 \ddot{T}_2 = 0, \tag{14}$$

where the first two equations represent the bending vibrations of two flexible links, and the last equation represents the torsional vibration of link 2. The boundary conditions are obtained not only from the natural conditions but also from geometric constraints [1]. The natural boundary conditions can be determined by gathering variations at boundaries and making them zero without regard to those variations, while the geometric boundary conditions are given in the kinematic level initially.

(a) *At* $x_2 = 0$: Since the rotary joint 1 is assumed clamped, there are three geometric constraints as follows:

$$y_2(0) = y_2'(0) = 0 \quad \text{and} \quad T_2(0) = 0. \tag{15}$$

(b) *At* $x_2 = L_2$ *or* $x_3 = 0$: The center mass is located in between two successive links so that the continuity of geometry and various force balance should be met.

$$y_2(L_2) = y_3(0), \tag{16}$$

$$y_2'(L_2) - T_2(L_2)\sin\theta_3 = y_3'(0), \tag{17}$$

$$EI_2 y_2''(L_2) = EI_3 y_3''(0) - I_c \ddot{y}_2'(L_2), \tag{18}$$

$$EI_2 y_2'''(L_2) = EI_3 y_3'''(0) + M_c \ddot{y}_2(L_2), \tag{19}$$

$$GJ_2 T_2'(L_2) = J_c \ddot{T}_2(L_2), \tag{20}$$

where the first two equations come from the geometric continuity of displacement and rotation, and the last three come from the natural boundary conditions, i.e., the bending moment, shear force, and torsional moment balances.

(c) *At* $x_3 = L_3$:

$$EI_3 y_3''(L_2) = -I_{tip} \ddot{y}_3'(L_3), \tag{21}$$

$$EI_3 y_3'''(L_2) = M_{tip} \ddot{y}_3(L_3), \tag{22}$$

where the first equation is the moment balance, and the second is the shear force balance at the tip.

Next we will derive the governing equations and boundary conditions when the joint boundary is assumed to be pinned–spring. The big difference is that we should include the effect of the rotation of joint 1 to $\mathscr{K}_0$ such that

$$\begin{aligned}\mathscr{K}_0 = {} & \tfrac{1}{2} J_1 \dot{\theta}_1^2 + \tfrac{1}{2} M_c (\dot{y}_2(L_2))^2 + \tfrac{1}{2} M_{tip} (\dot{y}_3(L_3))^2 + \tfrac{1}{2} I_c (\dot{y}_2'(L_2))^2 \\ & + \tfrac{1}{2} I_{tip} (\dot{y}_3'(L_3))^2 + \tfrac{1}{2} J_c (\dot{T}_2(L_2))^2,\end{aligned} \tag{23}$$

where J_1 is the rotary inertia of joint 1. The angular rotation of joint 1 is assumed to be small, and this assumption is reasonable when the robot's joint is controlled by stable controller. Under the assumption, we have the following trigonometric relation:

$$\theta_1 \sin\theta_2 = y_2'(0). \tag{24}$$

The kinetic energy from elastic links $\mathscr{K}_1$ and the potential energy $\mathscr{P}$ are the same as before in Eqs. (5) and (6). However, the non-conservative work is no longer zero; it should be

$$\delta \mathscr{W}_{nc} = \tau_1 \, \delta\theta_1 = \tau_1 \, \delta y_2'(0)/\sin\theta_2, \tag{25}$$

where τ_1 is the torque at joint 1. Suppose that the proportional control is the dominant servo action. Then, we can set $\tau_1 = -K_1\theta_1$, where K_1 is the proportional gain. It is interesting to investigate the effect of this gain, which will be shown later. We call this kind of boundary the pinned with spring condition [5] even though the spring is artificially given. Putting the kinetic energy in Eq. (23) and the non-conservative work in Eq. (25) into Eq. (2), we can obtain the governing equations and boundary conditions. Simply, the governing equations are the same as in Eqs. (12)–(14), whereas the boundary conditions at $y_2 = 0$ are different as follows:

$$\begin{aligned} &y_2(0) = 0, \quad T_2(0) = 0, \\ &EI_2 y_2''(0)\sin^2\theta_2 = K_1 y_2'(0) + J_1 \ddot{y}_2'(0). \end{aligned} \tag{26}$$

The underlying meaning of Eq. (26) is that the slope $y_2'(0)$ at the joint is being constrained by the spring while the elastic moment is acting on. If K_1 is large, the slope at the joint will remain very small as if it were clamped at the joint. On the contrary, if K_1 is small, then the slope of link will not be regulated well; it rather looks like a pinned boundary. The change of θ_2 also affects joint boundary condition. As $\sin^2\theta_2$ is fairly decreased, joint 1 becomes a heavier inertia and a larger servo gain actuator. Extremely, if θ_2 becomes zero, the bending moment at joint boundary cannot be exerted on the joint. If θ_2 is $\pi/2$, the bending moment is transferred directly to joint 1. Thus, K_1 and θ_2 are key parameters for the characteristics of pinned–spring boundary condition at joint 1. The other boundary conditions are the same as the previous development in Eqs. (16)–(22).

3.2. System mode analysis

In Eqs. (12)–(14), the governing equations of bending and torsion are decoupled from each other. However, those boundary conditions are mixed complicatedly, which makes bending and torsional vibrations depending on each other. In the system mode analysis, every vibration mode is solved together by combining all the conditions. This implies that each of the modal time functions is the common solution of all the participating bending and torsional vibrations. Consider m number of series solution of the bending vibration $y(x,t)$ that covers the entire domain:

$$y(x,t) = \begin{cases} y_2(x_2,t) = \sum_{j=1}^{m} \phi_j(x_2) q_j(t), & 0 \leqslant x = x_2 \leqslant L_2, \\ y_3(x_3,t) = \sum_{j=1}^{m} \psi_j(x_3) q_j(t), & 0 \leqslant x - L_2 = x_3 \leqslant L_3, \end{cases} \tag{27}$$

where ϕ_j and ψ_j are the jth system mode shapes of bending vibration for links 2 and 3, respectively, and q_j is the time function for the jth system mode. The bending vibration $y(x,t)$ is made by just patching y_2 and y_3, using the common time function q_j. This is because q_j represents the system mode of the whole system. It prevails in the whole domain of the horizontal vibration system. On the other hand, in the conventional component mode analysis, time functions should be defined differently in y_2 and y_3. Similarly, the series solution of torsional deflection in system

modes can be written as

$$T(x,t)=\begin{cases} T_2(x_2,t)=\sum_{j=1}^{m}\eta_j(x_2)q_j(t), & 0\leqslant x=x_2\leqslant L_2,\\ T_3(x_3,t),=0, & 0\leqslant x-L_3=x_3\leqslant L_3, \end{cases} \tag{28}$$

where η_j is the jth system mode shape for torsional vibration of link 2. Again, we use the same time function $q_j(t)$ because we are to solve the system modes mixed with every bending and torsional vibrations coupled with along the entire system. The torsional deflection at link 3 is set to identically zero as assumed in the beginning of this section. According to vibration theory, normal mode time solution can be written as

$$q_j(t)=\exp(\omega_j t), \tag{29}$$

where ω_j is the natural frequency of the jth system mode.

Substituting Eqs. (27)–(29) into Eqs. (12)–(14), the spatial solutions of bending vibration can be determined by the ordinary differential equations (ODEs) such that

$$\begin{aligned} &\phi_j''''(x_2)-\lambda_j^4\phi_j(x_2)=0,\\ &\psi_j''''(x_3)-\mu_j^4\psi_j(x_3)=0, \end{aligned} \tag{30}$$

and that of torsional vibration can be obtained by the second order ODE as

$$\eta_j''(x_2)+\kappa_j^2\eta_j(x_2)=0. \tag{31}$$

In the above, we defined that $\lambda_j^4\triangleq\rho_2\omega_j^2/EI_2$, $\mu_j^4\triangleq\rho_3\omega_j^2/EI_3$, and $\kappa_j^2\triangleq b_2\omega_j^2/GJ_2$, so it is satisfied that

$$\mu_j=\left(\frac{EI_2\,\rho_3}{EI_3\,\rho_2}\right)^{1/4}\lambda_j \quad\text{and}\quad \kappa_j=\left(\frac{EI_2\,b_2}{GJ_2\,\rho_2}\right)^{1/2}\lambda_j^2. \tag{32}$$

The general forms of the solutions of Eqs. (30) and (31) can be given by

$$\begin{aligned} \phi_j(x_2)&=A_1\sin(\lambda_j x_2)+B_1\sinh(\lambda_j x_2)+C_1\cos(\lambda_j x_2)+D_1\cosh(\lambda_j x_2),\\ \psi_j(x_3)&=A_2\sin(\mu_j x_3)+B_2\sinh(\mu_j x_3)+C_2\cos(\mu_j x_3)+D_2\cosh(\mu_j x_3),\\ \eta_j(x_2)&=A_3\sin(\kappa_j x_2)+B_3\cos(\kappa_j x_2). \end{aligned} \tag{33}$$

Introducing Eqs. (27)–(29) into boundary conditions, we can rewrite them in terms of spatial functions, i.e., $\phi_j(x_2),\psi_j(x_3)$, and $\eta_j(x_2)$. Furthermore, if the spatial solutions in Eq. (33) are substituted, we will get a set of linear homogeneous equations which are written in a linear matrix equation as

$$\mathbf{H}(\lambda)\mathbf{v}=\mathbf{0}, \tag{34}$$

where $\mathbf{v}=[A_1\ B_1\ C_1\ D_1\ A_2\ B_2\ C_2\ D_2\ A_3\ B_3]^{\mathrm{T}}$ is a vector of undetermined constant. Element by element expression of $\mathbf{H}(\lambda)$ is not provided due to space limitation, but it is straightforward to determine $\mathbf{H}(\lambda)$ without difficulty. The eigenvalues (or natural frequencies) of whole system can be determined from the frequency equation given by

$$\det(\mathbf{H}(\lambda))=0 \tag{35}$$

at the non-trivial solutions λ's. The closed form of $\det(\mathbf{H}(\lambda))$ is complex, so a symbolic package will be useful. The Macsyma[1] package was utilized in this paper to get $\mathbf{H}(\lambda)$ and its determinant in symbolic way. For determined solutions either symbolically or numerically, non-trivial $\mathbf{v}$'s, which are called eigenvectors, will be obtained in the null space of $\mathbf{H}(\lambda)$. These vectors determine the system mode shapes of the horizontal subsystem.

3.3. Orthogonal relations

By imposing all the boundary conditions on the governing equations, the orthogonal relations between mode shapes are obtained for both cases where joint 1 is modelled to be clamped and pinned–spring. These orthogonal relations will be useful in extracting mode shapes from the displacement data. We can also confirm the validity of the boundary conditions by deriving these relations.

(a) *Clamped at joint* 1: If joint 1 is clamped, the orthogonal relation is

$$\begin{aligned}&\int_0^{L_2} \rho_2\phi_i(x_2)\phi_j(x_2)\,\mathrm{d}x_2 + \int_0^{L_3} \rho_3\psi_i(x_3)\psi_j(x_3)\,\mathrm{d}x_3 + \int_0^{L_2} b_2\eta_i(x_2)\eta_j(x_2)\,\mathrm{d}x_2\\ &\quad + M_c\phi_i(L_2)\phi_j(L_2) + I_c\phi_i'(L_2)\phi_j'(L_2) + M_{tip}\psi_i(L_3)\psi_j(L_3)\\ &\quad + I_{tip}\psi_i'(L_3)\psi_j'(L_3) + J_c\eta_i(L_2)\eta_j(L_2) = 0 \quad \text{if } i\neq j. \end{aligned} \tag{36}$$

For the proof, see Appendix A.

(b) *Pinned–spring at joint* 1: If joint 1 is spring-hinged, the orthogonal relation is

$$\begin{aligned}&\int_0^{L_2} \rho_2\phi_i(x_2)\phi_j(x_2)\,\mathrm{d}x_2 + \int_0^{L_3} \rho_3\psi_i(x_3)\psi_j(x_3)\,\mathrm{d}x_3 + \int_0^{L_2} b_2\eta_i(x_2)\eta_j(x_2)\,\mathrm{d}x_2\\ &\quad + \frac{J_1}{\sin^2\theta_2}\phi_i'(0)\phi_j'(0) + M_c\phi_i(L_2)\phi_j(L_2) + I_c\phi_i'(L_2)\phi_j'(L_2) + M_{tip}\psi_i(L_3)\psi_j(L_3)\\ &\quad + I_{tip}\psi_i'(L_3)\psi_j'(L_3) + J_c\eta_i(L_2)\eta_j(L_2) = 0 \quad \text{if } i\neq j. \end{aligned} \tag{37}$$

For the proof, see Appendix A.

4. Numerical examples

The numerical examples illustrate how we can obtain the solutions of the system modes and what the results look like. The calculated natural frequencies and mode shapes will be compared according to the boundary condition at joint 1. The numerical values applied to a robot model are summarized in Table 1.

Modal frequencies: Assuming that joint 1 is clamped, the first three natural frequencies of horizontal vibration are summarized in Table 2 at various configurations. Roughly, the first mode is ranging from 1.7 to 2 Hz, while the second mode is ranging from 5 to 3 Hz as θ_3 varies from 0° to 90°. These two modes move reversely as θ_3 increases, and they are expected to be the same value when two links are folded exactly. To ascertain the effect of torsional coupling, we also investigate

[1] All rights reserved to Macsyma Inc.

Table 1
Physical parameters

Parameters	Symbol	Value
Length of link 2	L_2	0.52 (m)
Length of link 3	L_3	0.52 (m)
Mass of link 2	m_2	0.44 (kg)
Mass of link 3	m_3	0.16 (kg)
Center mass	M_c	1.58 (kg)
Mass of lumped tip	M_{tip}	0.29 (kg)
Inertia of joint 1	J_1	0.00932 (kg m^2)
Inertia of center mass	I_c	0.00365 (kg m^2)
Inertia of end tip mass	I_{tip}	0.0000293 (kg m^2)
Flexural rigidity of link 2	EI_2	24.4 (N m^2)
Flexural rigidity of link 3	EI_3	6.35 (N m^2)
Shear rigidity of link 2	GJ_2	17.23 (N m^2)

Table 2
Clamped joint

Elbow angle (θ_3) (deg)	f_1 (Hz)	f_2 (Hz)	f_3 (Hz)
0	1.7089	5.0604	16.9262
10	1.7152	4.9907	17.1548
20	1.7244	4.8009	17.6484
30	1.7420	4.5451	18.4020
40	1.7625	4.2581	19.2849
50	1.8299	3.9878	20.1884
60	1.8334	3.7478	20.8585
70	1.8848	3.5431	21.4025
80	1.9904	3.3306	21.7633
90	2.0271	3.2036	21.9361

the case where the torsional moment is neglected. The natural frequencies for this case are summarized in Table 3. If we compare these results, we can find out that torsional moment lowers the natural frequencies of the system. The effect of torsional moment becomes clear around $\theta_3 = 90^\circ$. We can conjecture the reason from the physical sense that the eccentricity by link 3 about the longitudinal axis of link 2 is maximized at $\theta_3 = 90^\circ$.

As another comparative work, the pinned–spring boundary condition at joint 1 is investigated. Table 4 shows its first three natural frequencies for different proportional gains and for different θ_3, while θ_2 is fixed to 90°. As the proportional gain K_1 becomes larger, the corresponding natural frequencies are increasing, and they approach to those of the ideal clamped natural frequencies. This result definitely supports the previous works from Refs. [5,6]. The effect of shoulder angle θ_2 on the natural mode is shown in Table 5. The values of K_1 and θ_3 are kept constant to 100 and 0°, and θ_2 is varied. As θ_2 becomes smaller, the first two natural modes are increased, but the third

Table 3
Clamped joint without torsion

Elbow angle (θ_3) (deg)	f_1 (Hz)	f_2 (Hz)	f_3 (Hz)
0	1.7123	5.0637	33.3751
10	1.7211	5.0513	33.3880
20	1.7469	5.0139	33.4521
30	1.7906	4.9480	33.5462
40	1.8520	4.8562	33.6835
50	1.9309	4.7347	33.8339
60	2.0271	4.5807	33.9781
70	2.1375	4.4012	34.0817
80	2.2626	4.1973	34.1011
90	2.3952	3.9782	34.0191

Table 4
Pinned–spring joint: ($\theta_2 = 90^\circ$)

Elbow angle (θ_3) (deg)	$K_1 = 50$			$K_1 = 100$			$K_1 = 300$		
	f_1 (Hz)	f_2 (Hz)	f_3 (Hz)	f_1 (Hz)	f_2 (Hz)	f_3 (Hz)	f_1 (Hz)	f_2 (Hz)	f_3 (Hz)
0	0.9970	4.0546	10.1475	1.2249	4.2670	11.0931	1.4997	4.6402	14.4143
10	0.9988	4.0063	10.1204	1.2257	4.2125	11.0773	1.5020	4.5791	14.3891
20	1.0080	3.8655	10.0441	1.2390	4.0471	11.0036	1.5119	4.4043	14.3316
30	1.0230	3.6624	9.9622	1.2556	3.8415	10.9179	1.5302	4.1648	14.2771
40	1.0433	3.4360	9.8807	1.2805	3.5990	10.8630	1.5577	3.8997	14.2282
50	1.0702	3.2102	9.8145	1.3142	3.3577	10.8143	1.5921	3.6398	14.2142
60	1.10101	3.0532	9.7648	1.3527	3.1378	10.7778	1.6372	3.4018	14.2000
70	1.1402	2.8256	9.7359	1.4004	2.9443	10.7536	1.6921	3.1924	14.1864
80	1.1821	2.679	9.7302	1.4565	2.7817	10.7354	1.7601	3.0126	14.1780
90	1.2257	2.5729	9.7013	1.5210	2.6536	10.7293	1.8410	2.8643	14.1752

mode is decreased. Considering the overall results, we are sure that the characteristics of the natural mode depend strongly on the boundary condition at joint 1. If it is clamped, the natural modes vary only according to the relative shape of two flexible links. If it is the pinned–spring, the natural modes are affected by the shoulder and elbow angles as well as controller gain.

Mode shapes: The mode shapes of horizontal vibration are very important in vibration suppression control since they provide the stable direction of controlled modes. Depending upon the joint boundary conditions and arm configurations, the mode shapes change considerably. Figs. 4 and 5 show the noticeable differences of mode shapes between clamped and pinned–spring joint conditions. To illustrate effectively, two links are depicted to lie on the horizontal plane in these figures. In the clamped joint case, the third mode is nearly stationary at the lumped mass positions, which is not the case in the pinned–spring condition. On the whole, every node in the mode shapes of the pinned–spring joint case appears in the middle of the flexible link.

Table 5
Effect of shoulder joint angle: ($K_1 = 100$, $\theta_3 = 0^\circ$)

Shoulder angle (θ_2) (deg)	f_1 (Hz)	f_2 (Hz)	f_3 (Hz)
10	1.6890	4.9479	7.0895
20	1.6180	4.7605	7.6310
30	1.5485	4.6000	8.3520
40	1.4445	4.4588	9.0500
50	1.3916	4.4100	9.7070
60	1.3220	4.3424	10.3511
70	1.2680	4.2880	10.7110
80	1.2308	4.2700	11.0030
90	1.2249	4.2670	11.0930

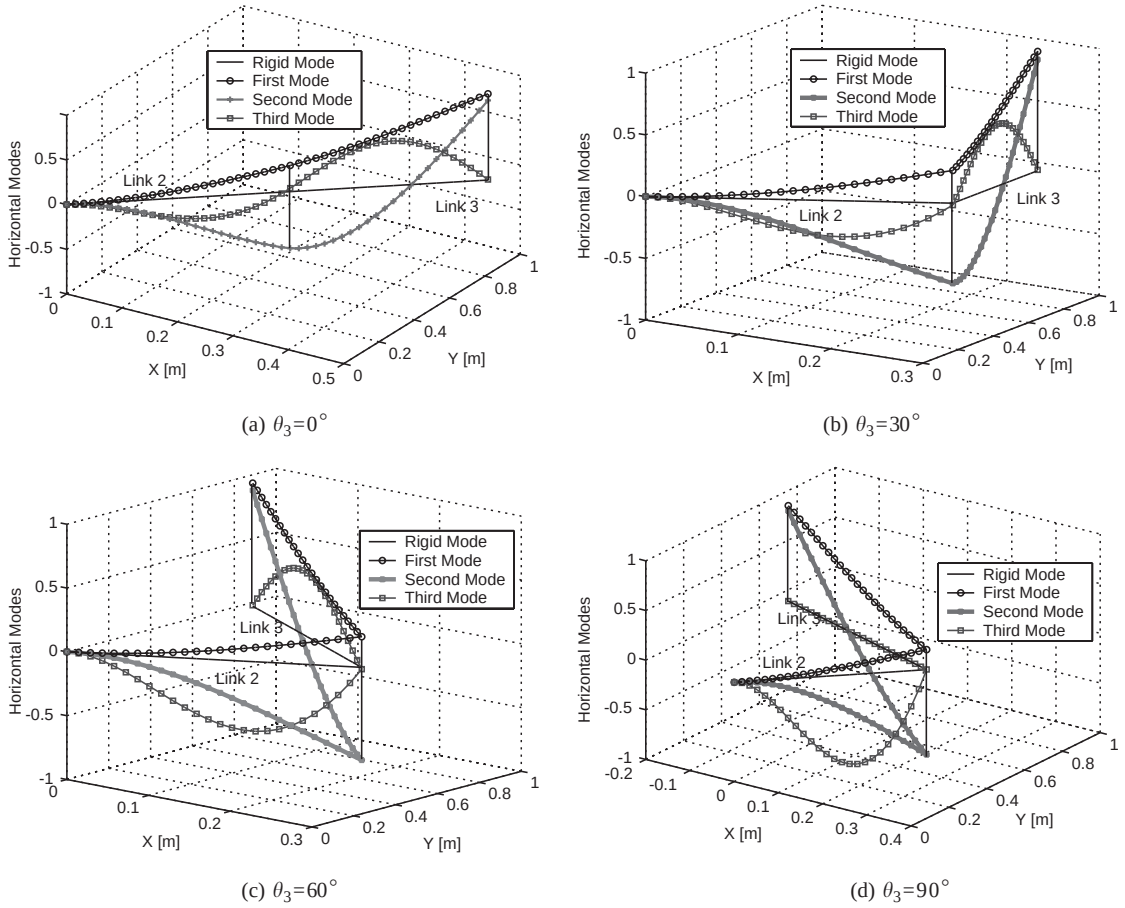

(a) θ_3=0° (b) θ_3=30°

(c) θ_3=60° (d) θ_3=90°

Fig. 4. Mode shapes of horizontal vibration: clamped.

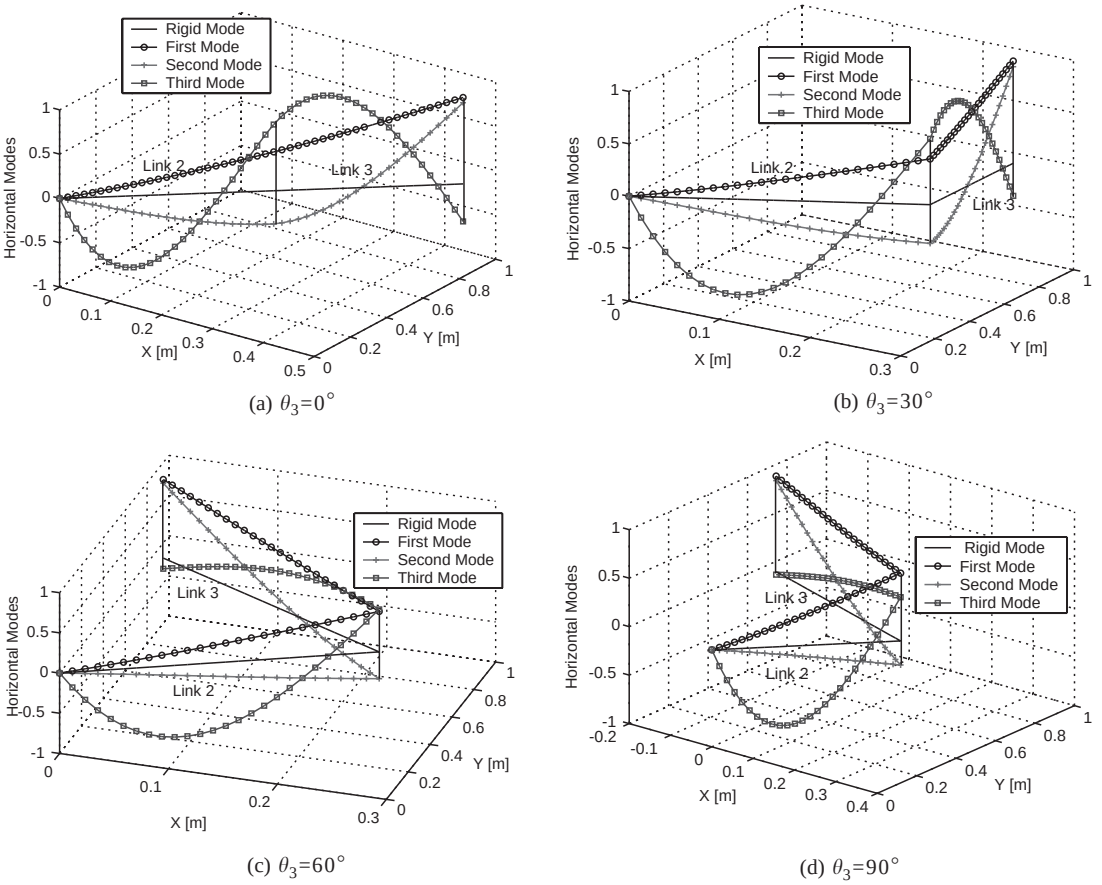

Fig. 5. Mode shapes of horizontal vibration: pinned–spring ($K_1 = 100, \theta_2 = 90°$).

5. Experimental verification

To verify the system mode analysis, we performed modal tests to the POSTECH flexible robot shown in Fig. 6. The robot has three joints and two flexible links. Each flexible link has circular cross-section and it is made of steel with high elasticity. The vibrations are measured by strain gauges attached at the sides of links. The physical parameters of the robot system is the same as Table 1. The natural frequencies of both clamped and pinned–spring boundary conditions were collected at various configurations using FFT technique. Then, they were compared with the numerically calculated results. For obtaining the natural frequencies of the clamped joint condition, we tightly locked joint 1 and exerted impact at the tip of robot. Table 6 illustrates the corresponding natural frequencies according to the variation of θ_3. As one can notice, the first two measured frequencies are very close to the numerical results in Table 2. FFT plots at four configurations are shown in Fig. 7. Due to the narrow bandwidth and low pass characteristic of our sensor system, high-frequency modes over the second mode were not visible. Table 7 shows

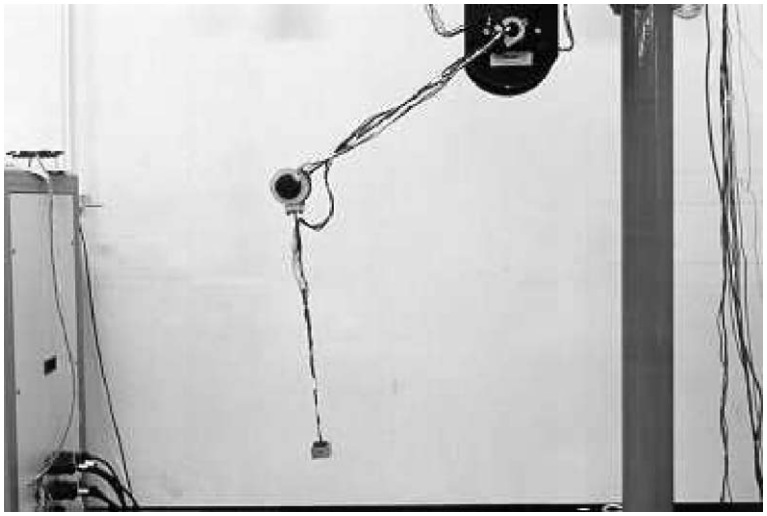

Fig. 6. Experimental system: POSTECH flexible robot.

Table 6
Clamped joint: experiment

Elbow angle (θ_3) (deg)	f_1 (Hz)	f_2 (Hz)
0	1.7090	5.1269
10	1.7090	5.1269
20	1.7090	4.8828
30	1.7090	4.6386
40	1.7090	4.3945
50	1.7090	4.0283
60	1.7090	3.7841
70	1.8310	3.5400
80	1.8310	3.4179
90	1.9531	3.2959

the first three natural frequencies for the pinned–spring boundary condition at joint 1 with different proportional gains. To implement the pinned–spring condition, the nonlinear friction in the joint was compensated dynamically. The compensated friction torque is mathematically modelled as

$$\tau_f = \tau_0 \operatorname{sgn}(\dot{\theta}_1) + K_f \dot{\theta}_1, \tag{38}$$

where τ_0 is Coulomb's friction, K_f is the viscous friction coefficient, and $\operatorname{sgn}(\cdot)$ is the signum function. Thus, the control torque in joint 1 was given by

$$\tau_1 = -K_p y_2'(0) + \tau_f, \tag{39}$$

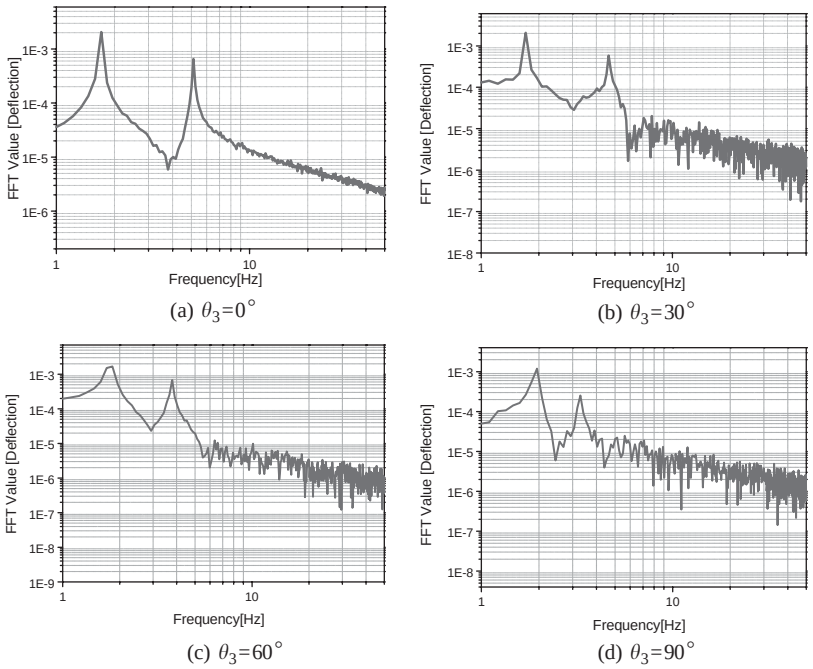

Fig. 7. FFT plots: clamped.

Table 7
Pinned–spring joint ($\theta_2 = 90°$): experiment

Elbow angle (θ_2) (deg)	$K_{p1} = 50$			$K_{p1} = 100$			$K_{p1} = 300$		
	f_1 (Hz)	f_2 (Hz)	f_3 (Hz)	f_1 (Hz)	f_2 (Hz)	f_3 (Hz)	f_1 (Hz)	f_2 (Hz)	f_3 (Hz)
0	1.0071	3.8452	7.8735	1.2817	4.2419	8.6975	1.4648	4.6692	11.3220
10	1.0376	3.7537	7.8430	1.2512	4.0894	8.4534	1.4648	4.5471	11.1694
20	1.0376	3.6011	7.7515	1.2817	3.9673	8.4534	1.4954	4.3945	11.1694
30	1.0681	3.4485	7.6599	1.3123	3.7537	8.3923	1.5258	4.1504	11.2000
40	1.0986	3.2959	7.5989	1.3428	3.5400	8.3618	1.5564	3.8757	11.1694
50	1.0986	3.1128	7.5378	1.3733	3.3264	8.3008	1.5869	3.6316	11.1694
60	1.1597	2.9297	7.5073	1.3733	3.3264	8.3008	1.6479	3.4180	11.3831
70	1.1902	2.7771	7.4768	1.4648	2.9297	8.2397	1.7090	3.2043	11.4746
80	1.2207	2.6245	7.4158	1.5259	2.777	8.2092	1.7700	3.0518	11.3831
90	1.2817	2.5330	7.3853	1.5869	2.6550	8.2092	1.8616	2.8992	11.3525

where the first term on the right hand side is the proportional servo action. While keeping the system closed, we applied an impulsive torque at joint 1 to initiate the vibration. Technically, a small amount of active damping was added to reduce chattering caused by friction compensation in Eq. (38). The recorded values in Table 7 are close to numerically calculated results in Table 4. As shown, larger proportional gain makes the natural frequencies larger. They will ultimately

approach to those of the clamped boundary condition for infinite gain. The FFT plot in Fig. 8 illustrates how the proportional gain affect the natural frequencies. Finally, in the pinned–spring joint, we verified the effect of the angle of the shoulder joint θ_2 to the natural frequencies. For different θ_2's, modal tests were performed, while K_1 and θ_3 were fixed to 100° and 0°. Fig. 9 shows the results after smoothing spikes of data. As θ_2 was increased, the first two natural frequencies were reduced. Meanwhile, the third mode was increased little by little, which matches well with the numerical results.

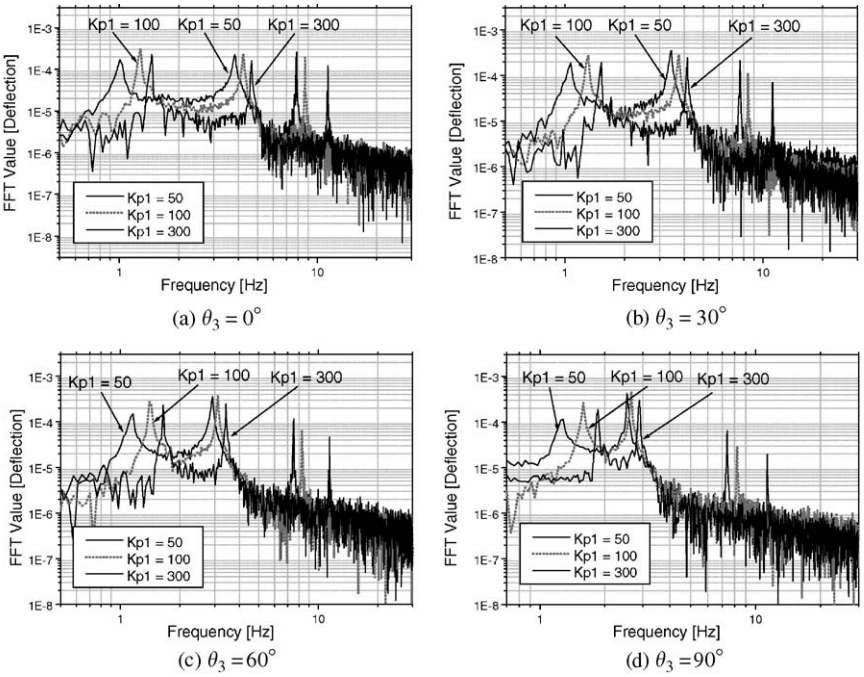

Fig. 8. FFT plots: pinned–spring ($\theta_2 = 90°$).

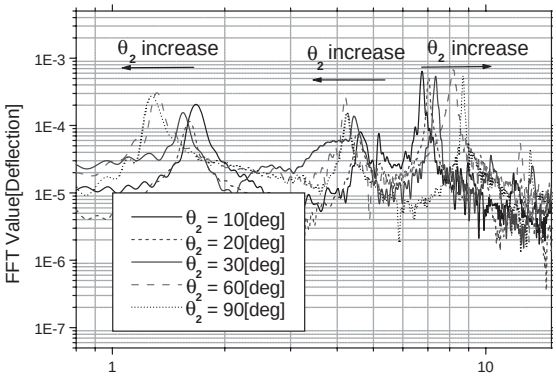

Fig. 9. Effect of the shoulder angle ($K_1 = 100, \theta_3 = 0°$).

6. Concluding remarks

The system mode analysis of horizontal vibration of a 3-D two-link flexible manipulator was investigated. To predict real systems more accurately, the mixed bending-torsional problem was formulated and analyzed using the extended Hamilton's principle. Without torsion modelling, the results would fail to precisely anticipate the actual horizontal vibration. The associated complex boundary conditions were derived, and their validity was confirmed. Depending on the modelling of boundary condition at joint 1, the modal frequencies and mode shapes underwent large change. In the pinned–spring joint model, the proportional gain and configurations were the key parameters for determining the natural frequencies. On the other hand, in the clamped joint model, the natural frequencies were affected only by the relative configuration of two flexible links. Through numerical and experimental studies, we verified the validity of our analysis. The analysis results can be applied to flexible structures in combination with bending and torsional vibration.

Appendix A

Proof of Eq. (36). From Eqs. (30) and (31), it can be written that

$$\int_0^{L_2} EI_2\lambda_i^4\phi_i(x_2)\phi_j(x_2)\,dx_2 + \int_0^{L_3} EI_3\mu_i^4\psi_i(x_3)\psi_j(x_3)\,dx_3 + \int_0^{L_2} GJ_2\kappa_i^2\eta_i(x_2)\eta_j(x_2)\,dx_2$$
$$= \int_0^{L_2} EI_2\phi_i''''(x_2)\phi_j(x_2)\,dx_2 + \int_0^{L_3} EI_3\psi_i''''(x_3)\psi_j(x_3)\,dx_3 - \int_0^{L_2} GJ_2\eta_i''(x_2)\eta_j(x_2)\,dx_2. \quad (A.1)$$

Applying the integration by part and putting condition in Eq. (15), the right hand side of Eq. (A.1) becomes

$$\int_0^{L_2} EI_2\phi_i''(x_2)\phi_j''(x_2)\,dx_2 + \int_0^{L_3} EI_3\psi_i''(x_3)\psi_j''(x_3)\,dx_3 + \int_0^{L_2} GJ_2\eta_i'(x_2)\eta_j'(x_2)\,dx_2$$
$$+ EI_2\phi_i'''(L_2)\phi_j(L_2) - EI_2\phi_i'''(L_2)\phi_j'(L_2) + EI_3\psi_i'''(L_3)\psi_j(L_3) - EI_3\psi_i'''(0)\psi_j(0)$$
$$- EI_3\psi_i''(L_3)\psi_j'(L_3) + EI_3\psi_i''(0)\psi_j'(0) - GJ_2\eta_i'(L_2)\eta_j(L_2).$$

Imposing the boundary conditions in Eqs. (16)–(22), we can get

$$\int_0^{L_2} EI_2\lambda_i^4\phi_i(x_2)\phi_j(x_2)\,dx_2 + \int_0^{L_3} EI_3\mu_i^4\psi_i(x_3)\psi_j(x_3)\,dx_3 + \int_0^{L_2} GJ_2\kappa_i^2\eta_i(x_2)\eta_j(x_2)\,dx_2$$
$$= \int_0^{L_2} EI_2\phi_i''(x_2)\phi_j''(x_2)\,dx_2 + \int_0^{L_3} EI_3\psi_i''(x_3)\psi_j''(x_3)\,dx_3 + \int_0^{L_2} GJ_2\eta_i'(x_2)\eta_j'(x_2)\,dx_2$$
$$- \omega_i^2 M_c\phi_i(L_2)\phi_j(L_2) + EI_3\psi_i'''(0)\phi_j(L_2) - \cos\theta_3 EI_3\psi_i''(0)\phi_j'(L_2) - \omega_i^2 I_{c,y}\phi_i'(L_2)\phi_j'(L_2)$$
$$- M_{tip}\omega_i^2\psi_i(L_3)\psi_j(L_3) - EI_3\psi_i'''(0)\psi_j(0) - I_{tip}\omega_i^2\psi_i'(L_3)\psi_j'(L_3)$$
$$+ EI_3\psi_i''(0)\psi_j'(0) + \sin\theta_3 EI_3\psi_i''(0)\eta_j(L_3) - \omega_i^2 I_{c,x}\eta_i(L_2)\eta_j(L_2). \quad (A.2)$$

Especially, introducing $\phi_j'(L_2) - \sin\theta_3\eta_j(L_2) = \psi_j'(0)$ and $\phi_j(L_2) = \psi_j(0)$ in Eqs. (16) and (17) into the above equation, it becomes

$$\begin{aligned}
&\omega_i^2 \int_0^{L_2} \rho_2\phi_i(x_2)\phi_j(x_2)\,\mathrm{d}x_2 + \omega_i^2 \int_0^{L_3} \rho_3\psi_i(x_3)\psi_j(x_3)\,\mathrm{d}x_3 + \omega_i^2 \int_0^{L_2} b_2\eta_i(x_2)\eta_j(x_2)\,\mathrm{d}x_2 \\
&\quad = \int_0^{L_2} EI_2\phi_i''(x_2)\phi_j''(x_2)\,\mathrm{d}x_2 + \int_0^{L_3} EI_3\psi_i''(x_3)\psi_j''(x_3)\,\mathrm{d}x_3 + \int_0^{L_2} GJ_2\eta_i'(x_2)\eta_j'(x_2)\,\mathrm{d}x_2 \\
&\qquad - \omega_i^2(M_c\phi_i(L_2)\phi_j(L_2) + I_{c,y}\phi_i'(L_2)\phi_j'(L_2) + M_{tip}\psi_i(L_3)\psi_j(L_3) \\
&\qquad + I_{tip}\psi_i'(L_3)\psi_j'(L_3) + I_{c,x}\eta_i(L_2)\eta_j(L_2)).
\end{aligned} \tag{A.3}$$

Similarly, if we exchange i and j, it becomes

$$\begin{aligned}
&\omega_j^2 \int_0^{L_2} \rho_2\phi_j(x_2)\phi_i(x_2)\,\mathrm{d}x_2 + \omega_j^2 \int_0^{L_3} \rho_3\psi_j(x_3)\psi_i(x_3)\,\mathrm{d}x_3 + \omega_j^2 \int_0^{L_2} b_2\eta_j(x_2)\eta_i(x_2)\,\mathrm{d}x_2 \\
&\quad = \int_0^{L_2} EI_2\phi_j''(x_2)\phi_i''(x_2)\,\mathrm{d}x_2 + \int_0^{L_3} EI_3\psi_j''(x_3)\psi_i''(x_3)\,\mathrm{d}x_3 + \int_0^{L_2} GJ_2\eta_j'(x_2)\eta_i'(x_2)\,\mathrm{d}x_2 \\
&\qquad - \omega_j^2(M_c\phi_j(L_2)\phi_i(L_2) + I_{c,y}\phi_j'(L_2)\phi_i'(L_2) + M_{tip}\psi_j(L_3)\psi_i(L_3) \\
&\qquad + I_{tip}\psi_j'(L_3)\psi_i'(L_3) + I_{c,x}\eta_j(L_2)\eta_i(L_2)).
\end{aligned} \tag{A.4}$$

By subtracting Eq. (A.4) from Eq. (A.3), we have

$$\begin{aligned}
0 = (\omega_i^2 - \omega_j^2)\Bigg(&\int_0^{L_2} \rho_2\phi_i(x_2)\phi_j(x_2)\,\mathrm{d}x_2 + \int_0^{L_3} \rho_3\psi_i(x_3)\psi_j(x_3)\,\mathrm{d}x_3 \\
&+ \int_0^{L_2} b_2\eta_i(x_2)\eta_j(x_2)\,\mathrm{d}x_2 M_c\phi_i(L_2)\phi_j(L_2) + I_{c,y}\phi_i'(L_2)\phi_j'(L_2) \\
&+ M_{tip}\psi_i(L_3)\psi_j(L_3) + I_{tip}\psi_i'(L_3)\psi_j'(L_3) + I_{c,x}\eta_i(L_2)\eta_j(L_2)\Bigg).
\end{aligned} \tag{A.5}$$

Since, $\omega_i^2 \neq \omega_j^2$ for $i \neq j$, the second parenthesized term must be zero, which concludes the proof. □

Proof of Eq. (37). Similar to clamped case, from Eqs. (30) and (31), it can be written that

$$\begin{aligned}
&\int_0^{L_2} EI_2\lambda_i^4\phi_i(x_2)\phi_j(x_2)\,\mathrm{d}x_2 + \int_0^{L_3} EI_3\mu_i^4\psi_i(x_3)\psi_j(x_3)\,\mathrm{d}x_3 + \int_0^{L_2} GJ_2\kappa_i^2\eta_i(x_2)\eta_j(x_2)\,\mathrm{d}x_2 \\
&\quad = \int_0^{L_2} EI_2\phi_i''''(x_2)\phi_j(x_2)\,\mathrm{d}x_2 + \int_0^{L_3} EI_3\psi_i''''(x_3)\psi_j(x_3)\,\mathrm{d}x_3 - \int_0^{L_2} GJ_2\eta_i''(x_2)\eta_j(x_2)\,\mathrm{d}x_2.
\end{aligned} \tag{A.6}$$

Applying the integration by part and introducing condition that $\phi_j(0) = 0$, the right hand side of the Eq. (A.6) becomes

$$\begin{aligned}
&\int_0^{L_2} EI_2\phi_i''(x_2)\phi_j''(x_2)\,\mathrm{d}x_2 + \int_0^{L_3} EI_3\psi_i''(x_3)\psi_j''(x_3)\,\mathrm{d}x_3 + \int_0^{L_2} GJ_2\eta_i'(x_2)\eta_j'(x_2)\,\mathrm{d}x_2 \\
&\quad + EI_2\phi_i'''(L_2)\phi_j(L_2) - EI_2\phi_i''(L_2)\phi_j'(L_2) + EI_2\phi_i''(0)\phi_j'(0) + EI_3\psi_i'''(L_3)\psi_j(L_3) \\
&\quad - EI_3\psi_i'''(0)\psi_j(0) - EI_3\psi_i''(L_3)\psi_j'(L_3) + EI_3\psi_i''(0)\psi_j'(0) - GJ_2\eta_i'(L_2)\eta_j(L_2).
\end{aligned}$$

Imposing the boundary conditions in Eqs. (16)–(22), and (26), we can get

$$\begin{aligned}
&\int_0^{L_2} EI_2\lambda_i^4\phi_i(x_2)\phi_j(x_2)\,dx_2 + \int_0^{L_3} EI_3\mu_i^4\psi_i(x_3)\psi_j(x_3)\,dx_3 + \int_0^{L_2} GJ_2\kappa_i^2\eta_i(x_2)\eta_j(x_2)\,dx_2\\
&\quad= \int_0^{L_2} EI_2\phi_i''(x_2)\phi_j''(x_2)\,dx_2 + \int_0^{L_3} EI_3\psi_i''(x_3)\psi_j''(x_3)\,dx_3 + \int_0^{L_2} GJ_2\eta_i'(x_2)\eta_j'(x_2)\,dx_2\\
&\quad\quad- \omega_i^2 M_c\phi_i(L_2)\phi_j(L_2) + EI_3\psi_i'''(0)\phi_j(L_2) + \frac{K_1}{\sin^2\theta_2}\phi_i'(0)\phi_j'(0) - \omega_i^2\frac{J_1}{\sin^2\theta_2}\phi_i'(0)\phi_j'(0)\\
&\quad\quad- \cos\theta_3 EI_3\psi_i''(0)\phi_j'(L_2) - \omega_i^2 I_{c,y}\phi_i'(L_2)\phi_j'(L_2) - \omega_i^2 M_{tip}\psi_i(L_3)\psi_j(L_3) - EI_3\psi_i'''(0)\psi_j(0)\\
&\quad\quad- \omega_i^2 I_{tip}\psi_i'(L_3)\psi_j'(L_3) + EI_3\psi_i''(0)\psi_j'(0) + \sin\theta_3 EI_3\psi_i''(0)\eta_j - \omega_i^2 I_{c,x}\eta_i(L_2)\eta_j(L_2). \qquad (A.7)
\end{aligned}$$

Further, introducing $\phi_j'(L_2) - \sin\theta_3\eta_j(L_2) = \psi_j'(0)$ and $\phi_j(L_2) = \psi_j(0)$ into the above equation, it becomes

$$\begin{aligned}
&\omega_i^2\int_0^{L_2}\rho_2\phi_i(x_2)\phi_j(x_2)\,dx_2 + \omega_i^2\int_0^{L_3}\rho_3\psi_i(x_3)\psi_j(x_3)\,dx_3 + \omega_i^2\int_0^{L_2} b_2\eta_i(x_2)\eta_j(x_2)\,dx_2\\
&\quad= \int_0^{L_2} EI_2\phi_i''(x_2)\phi_j''(x_2)\,dx_2 + \int_0^{L_3} EI_3\psi_i''(x_3)\psi_j''(x_3)\,dx_3 + \int_0^{L_2} GJ_2\eta_i'(x_2)\eta_j'(x_2)\,dx_2\\
&\quad\quad- \omega_i^2\left(\frac{J_1}{\sin^2\theta_2}\phi_i'(0)\phi_j'(0) + M_c\phi_i(L_2)\phi_j(L_2) + I_{c,y}\phi_i'(L_2)\phi_j'(L_2) + M_{tip}\psi_i(L_3)\psi_j(L_3)\right.\\
&\quad\quad\left.+ I_{tip}\psi_i'(L_3)\psi_j'(L_3) + I_{c,x}\eta_i(L_2)\eta_j(L_2)\right) + \frac{K_1}{\sin^2\theta_2}\phi_i'(0)\phi_j'(0). \qquad (A.8)
\end{aligned}$$

In the above, different from the proof of Eq. (A.3), a term related with servo gain is appeared, though it will be cancelled and dropped out. If we exchange i and j, it becomes

$$\begin{aligned}
&\omega_j^2\int_0^{L_2}\rho_2\phi_j(x_2)\phi_i(x_2)\,dx_2 + \omega_j^2\int_0^{L_3}\rho_3\psi_j(x_3)\psi_i(x_3)\,dx_3 + \omega_j^2\int_0^{L_2} b_2\eta_j(x_2)\eta_i(x_2)\,dx_2\\
&\quad= \int_0^{L_2} EI_2\phi_j''(x_2)\phi_i''(x_2)\,dx_2 + \int_0^{L_3} EI_3\psi_j''(x_3)\psi_i''(x_3)\,dx_3 + \int_0^{L_2} GJ_2\eta_j'(x_2)\eta_i'(x_2)\,dx_2\\
&\quad\quad- \omega_j^2\left(\frac{J_1}{\sin^2\theta_2}\phi_j'(0)\phi_i'(0) + M_c\phi_j(L_2)\phi_i(L_2) + I_{c,y}\phi_j'(L_2)\phi_i'(L_2) + M_{tip}\psi_j(L_3)\psi_i(L_3)\right.\\
&\quad\quad\left.+ I_{tip}\psi_j'(L_3)\psi_i'(L_3) + I_{c,x}\eta_j(L_2)\eta_i(L_2)\right) + \frac{K_1}{\sin^2\theta_2}\phi_j'(0)\phi_i'(0). \qquad (A.9)
\end{aligned}$$

By subtracting Eq. (A.9) from Eq. (A.8), we have

$$\begin{aligned}
0 = (\omega_i^2 - \omega_j^2)&\left(\int_0^{L_2}\rho_2\phi_i(x_2)\phi_j(x_2)\,dx_2 + \int_0^{L_3}\rho_3\psi_i(x_3)\psi_j(x_3)\,dx_3 + \int_0^{L_2} b_2\eta_i(x_2)\eta_j(x_2)\,dx_2\right.\\
&+ \frac{J_1}{\sin^2\theta_2}\phi_j'(0)\phi_i'(0) + M_c\phi_i(L_2)\phi_j(L_2) + I_{c,y}\phi_i'(L_2)\phi_j'(L_2)\\
&\left.+ M_{tip}\psi_i(L_3)\psi_j(L_3) + I_{tip}\psi_i'(L_3)\psi_j'(L_3) + I_{c,x}\eta_i(L_2)\eta_j(L_2)\right). \qquad (A.10)
\end{aligned}$$

Since, $\omega_i^2 \neq \omega_j^2$ for $i \neq j$, the second parenthesized term must be zero, which concludes the proof. □

References

[1] C.M. Oakley, Experiments in Modeling and End-point Control of Two-link Flexible Manipulators. Ph.D. Thesis, Stanford University, 1991.
[2] H. Bang, Analytical solution for dynamic analysis of a flexible l-shaped structure, Journal of Guidance 19 (1996) 248–250.
[3] R.I. Milford, S.F. Asokanthan, Configuration dependent eigenfrequencies for a two-link flexible manipulator: Experimental verification, Journal of Sound and Vibration 222 (2) (1999) 191–207.
[4] J. Cheong, Y. Youm, W.K. Chung, Investigation and comparison of possible boundary conditions and system vibration modes in two-link flexible manipulators, in: Proceedings of the ASME International Symposium on Advances in Robot Dynamics and Control, IMECE, vol. CD-2, 2001.
[5] E. Garcia, D.J. Inman, Modeling of the slewing control of a flexible structure, Journal of Guidance 14 (4) (1991) 736–742.
[6] S. Cetinkunt, W.-L. Yu, Closed-loop behavior of a feedback-controlled flexible arm: a comparative study, International Journal of Robotics Research 10 (1991) 263–275.
[7] T. Yoshikawa, H. Murakami, K. Hosoda, Modeling and control of a three degree of freedom manipulator with two flexible links, in: Proceedings of the 29th Conference on Decision and Control, 1990, pp. 2532–2537.
[8] Y. Sakawa, Z.H. Luo, Modeling and control of coupled bending and torsional vibrations of flexible beams, IEEE Transactions on Automatic Control 34 (1989) 970–977.
[9] L. Chen, N.G. Chalhoub, Modeling and control of transverse and torsional vibration in a spherical robotic manipulator: theoretical and experimental results, Transactions of the American Society of Mechanical Engineers Journal of Dynamic Systems Measurements and Control 119 (1997) 421–430.
[10] L. Meirovitch, Analytical Methods in Vibrations, Macmillan Company, New York, 1967.